Bi-Material 3D Printed Soft Microrobots: Proof-of-Concept and Demonstration

Mehdi Salah[1], Yannis Bordes[1], Cédric Clévy[1], Gwenn Ulliac[1], Vincent Luzet[1], Adam Chafai[2], Muamer Kadic[1], Pierre Lambert[2], and Kanty Rabenorosoa[1]

***Abstract*— This paper proposes to investigate a bi-material approach that introduces another material in the 3D printed soft microrobot working as a structural skeleton of the active material. For the latter, pNIPAM-based hydrogels are good candidates thanks to their large deformation under stimuli. However, this same property is a trade-off with mechanical strength, and by extension the structural stability of the printed microrobots. By combining two materials, the shortcomings of one can be palliated by the second material. Here, we propose to make 3D 100µm-scale tethered microrobots with pNIPAM beams as an actuator into IP-S flexible mechanisms, using bi-material 2-Photon Polymerization (2PP) printing as a fabrication process. The capacity of the pNIPAM beams as actuators is studied experimentally and via Finite Element Modelling, revealing promising capacities in displacement and forces during simulations (contraction up to 25%, force up to 166 µN). The behavior of pNIPAM-actuated IP-S flexible mechanisms is explored in a 2PP-printed microrobot, demonstrating a state-of-the-art motion range (joint rotation up to 14°) easily controllable by temperature change. Furthermore, actuated 3D mechanisms are demonstrated with three 100µm 3D grippers.**

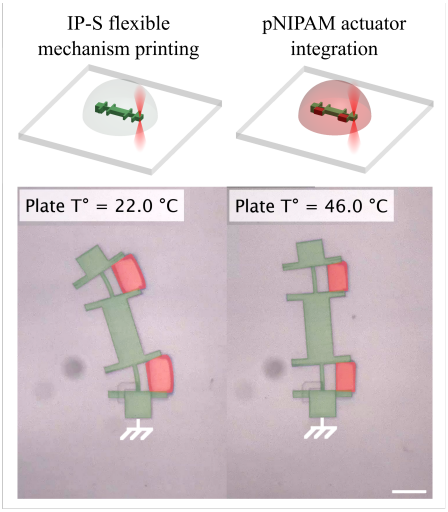

Fig. 1: 3D printed bi-material soft microrobot composed of a flexible mechanism in IP-S (highlighted in green) and two pNIPAM actuators (highlighted in red), and it's actuation when heated between 22°C and 46°C. Scale bar : 50µm

I. INTRODUCTION

Nowadays, robots are used to achieve tasks at the micro-nanoscale in various domains [1], [2], [3], [4], [5]. However, these robots used for movement with micrometric resolution have dm-scale sizes, and this causes several problems. Especially, it adds a major constraint on the robotic system: to execute a task at the µm scale, an enormous free space is needed to ensure that the tool can access the part of the workspace where the task is executed. Thus, confined spaces are out of reach for these robots without tearing them apart.

One way to bring robots into those spaces would be to reduce their scale. Several miniaturized robots have been proposed at the centimeter scale [6], [7] [8], [9], [10], and at the millimeter scale [11], [12], [13] which have demonstrated real advancements for microrobotic tasks. However, their downscaling effort has been so far limited by the actuators used in the mechanism (use of standard components like piezoelectric actuators [6], [**?**], limitations of actual MEMS actuators [10], [12]) or of the manufacturing techniques used to produce the robot [10], [13].

Many approaches are currently investigated to reduce the scale of robots even further. Among them, one of particular interest is to use 2-Photon Polymerization (2PP), a 3D printing technique capable to make µm-scale structures with resolution up to 120 nm [14]. Especially, 4D printing approaches are investigated, with active materials actuated via diverse stimuli, to make active devices in several application fields [15] like microrobotics [16].

Active hydrogels, like poly(N-isopropylacrylamide) (pNIPAM) based or bovine serum albumin (BSA)

This work was supported by the regional Bourgogne Franche-Comté project NanoFolding, the EIPHI Graduate School (contract "ANR-17-EURE-0002"), the French RENATECH network through its FEMTO-ST technological facility, the Equipex CMNR and the ANR PNanoBot (contract "ANR-21-CE33-0015").

[1]Authors are with FEMTO-ST Institute, Univ. Bourgogne Franche-Comté, CNRS, 15B avenue des Montboucons, 25030 Besançon, cedex, France. mehdi.salah@femto-st.fr, kanty.rabenorosoa@femto-st.fr

[2]Pierre Lambert and Adam Chafai are with Transfers Interfaces and Processes (TIPs), Université Libre de Bruxelles, Av. Franklin Roosevelt 50, 1050 Brussels, Belgium pierre.lambert@ulb.be

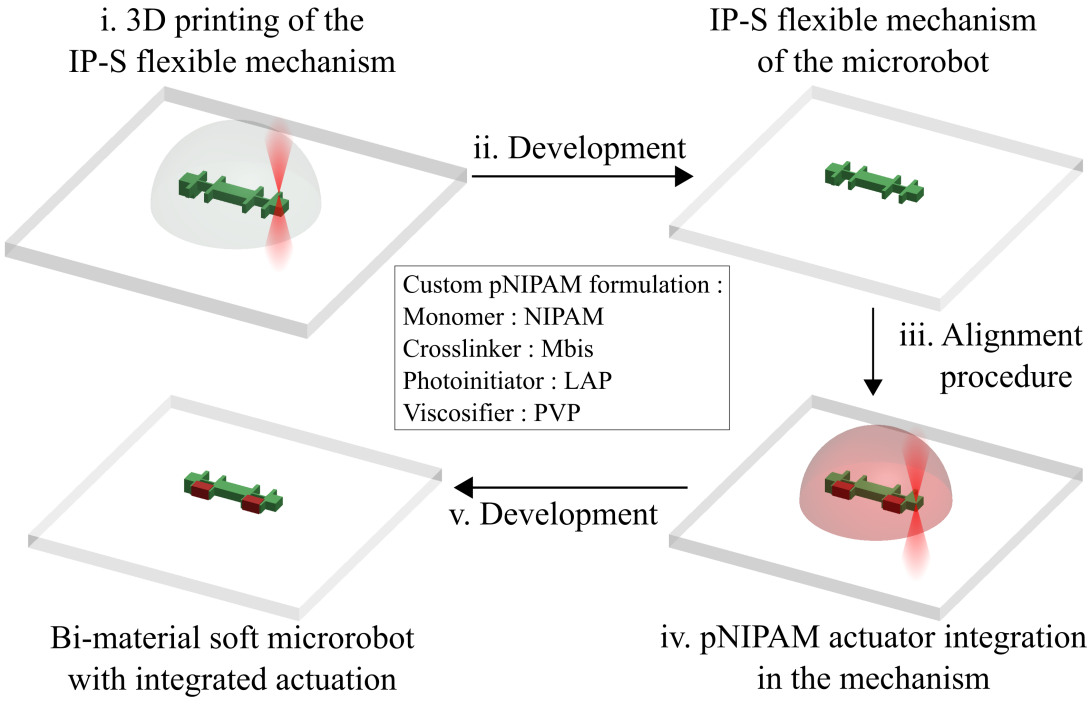

Fig. 2: Description of the fabrication process for IP-S/pNIPAM bi-material microrobots: (i) Step 1 - Fabrication of the IP-S flexible mechanism, (ii) Step 2 - Development of the IP-S resin, (iii) Step 3 - Alignment procedure on cross markers printed beforehand to prepare the next step (iv) Step 4 - pNIPAM actuator printing onto the IP-S mechanism, (v) Step 5 - Development of the pNIPAM.

based hydrogel, are active materials with important shrinkage when submitted to the appropriate stimulus, a very useful property to generate large movement on demand. Indeed, it has been used in many microdevices fabricated with 2PP printing, responding to various stimuli like pH [17], [18], temperature [19], [20] or light [21], [22], [23].

However, the previously cited devices have been made with only one material: an active hydrogel. This means that the same set of properties are inherited across the entire device: low printability [20], low Young Modulus [24], [25], isotropic shrinkage, stimulus-responsiveness, etc. But a microrobot cannot be homogeneous, it need "parts": to generate meaningful movement beyond shrinkage, symmetry need to be broken in the device by parts with different behaviors [26]; and to have multi-DoF microrobots, parts of the robot need to be actuated differently and independently. If the device is made in only one material, the methods left to make parts are geometry, Graytone lithography and chemical functionalization. Problem: the first method is limited by the low fabricability of active hydrogels [20], the second method only allow quantitative change in the properties set [20], and the third one can at most add a property in the structure [27]. Thus, the fabricated active devices are heavily limited by their base material.

One way to solve this problem would be to combine several materials with complementary properties, each one assuming a different role in the microrobot. This approach was used in 2PP-printed structures like [28], [29], [30] and [31] to add new functionalities with hard and soft parts. In particular, it was used in [32] [33] and [34] to create a structural skeleton for an active hydrogel, generating movement with the hydrogel contraction.

This bi-material approach has yet to be investigated in the case of soft tethered microrobots. Herein, 3D 100-µm scale microrobots are made via a straightforward bi-material 2PP printing approach (Fig. 1). The interest of the bi-material approach is demonstrated by the fabrication of 3D microrobots, and the large and controllable actuation observed relatively to temperature. In section II of this work, the chosen design approach is explained, the 2-step printing process employed in this work is presented and the FEM model used in this work is stated. Section III proposes a static characterization of the pNIPAM actuator, based on a free displacement experiment and finite element modelling of the response under load. Then in section IV, fabrication of 100-µm scale IP-S mechanism with integrated pNIPAM actuators is reported. Large displacement comparable to the state-of-the-art and controllable according to temperature is achieved in a RR microrobot. Finally, as a proof of concept for 3D actuated mechanisms, 100 µm-scale actuated grippers

are fabricated and actuated.

II. METHODS

A. Choices of design

To obtain large deformation with bimaterial 2PP-printed structures, designs combining flexible mechanism made in a passive material and actuators made in an active material were introduced. The mechanisms were designed in the framework of compliant mechanism [35]. This methodology allows to make monolithic structures able to withstand themselves during printing while defining a kinematic architecture with controlled degrees of freedom. pNIPAM beams were used as actuators to apply a uniaxial force on the mechanism. The beam geometry was chosen because the flexible mechanism only needed a source of deformation, while the guidance of the movement was assured by the mechanism itself. For the flexible mechanism, IP-S was chosen thanks to its good printability at the 100 µm scale and its high rigidity which allowed to make slender yet still robust structures. It was combined with pNIPAM, chosen as an actuator thanks to its large deformation when heated around its Lower Critical Solution Temperature (LCST) [19] [20]. Also, these two polymers have methacrylate and acrylamide groups as their monomer's reactive groups, hinting to a good chemical adhesion between the two, a fact of paramount importance when printing hybrid structures. The good adhesion was later confirmed in the fabricated structures.

B. Fabrication process

The pNIPAM actuators were printed with a custom resin. The formulation used was adapted from [19], with N-isopropylacrylamide (NIPAM) (Sigma-Aldrich, ≥99%) as a monomer, N,N'-methylenebis(acrylamide) (Mbis) (Sigma-Aldrich, ≥99.5%) as crosslinker, lithium phenyl(2,4,6-trimethylbenzoyl)phosphinate (LAP) (TCI Tokyo Chemical Industry, >98%) as photoinitiator and ethylene glycol (Sigma-Aldrich, >99%) as solvent. Polyvinylpyrrolidone (PVP) (Thermo Scientific Chemicals, Average M.W. 1.300.000, K85-95) was added to improve the viscosity of the resin, and thus its printability [20]. An IP-S commercial resin from Nanoscribe GmbH was used to print the flexible mechanisms.

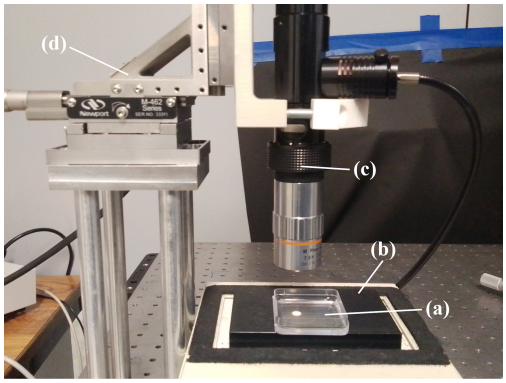

Fig. 3: The global heating experimental setup, with (a) the sample in its water bath, (b) the heating/cooling plate, (c) the microscope, and (d) the XYZ stage.

The fabrication of the devices was done with a 2-step 2PP printing process similar to [31] (Fig. 2), using a 25 ×, NA= 0.8 objective in the oil immersion configuration for the two materials. The IP-S flexible mechanism was printed first to act as support for the actuators, using the default parameters for IP-S solid parts. When large overhangs parallel to the substrate plane were needed, a small stitching strategy was used [36]. For each printed mechanism, a cross marker was printed at the origin of the printing job to align the actuator printing job in the second step. After developing the IP-S resin out of the 3D printer, the substrate was reinserted with pNIPAM resin placed on the IP-S structures. The angular alignment of the substrate in the substrate holder was done manually with a mark graved on the substrate before the first impression step. The alignment of the actuators with the passive mechanism was done using the previously printed cross markers. The pNIPAM actuators were printed with a 50mW laser power, a 20 kµm/s scan speed, a slicing distance of 1 µm and a hatching distance of 0.2 µm. When the pNIPAM actuator fabrication was done, the devices were developed in several baths of IPA and deionized water, and then stored in deionized water. A visual check under an optical microscope was done after each printing step.

C. Material model used for pNIPAM in the Finite Element Model

Finite Element Modelling with COMSOL Multiphysics was used to study the force generated by the pNIPAM actuator. In the model, pNIPAM is considered as a linear elastic material with an isotropic thermal contraction. Thermal strain and Young modulus were dependent on the temperature. The phenomenological model proposed by Puleo et al. [37] was used to describe the evolution of the Young modulus and thermal contraction of the pNIPAM according to temperature with equation (1), (2) and (3).

The mechanical properties of the pNIPAM were expressed relatively to the swollen state, with the pNIPAM state at T_0 = 22°C considered as reference. The equation (1), modelling the relative volumic ratio $\frac{V(T_0)}{V(T)}$ with respect to the pNIPAM temperature T as a sigmoidal law, is used as a constitutive law of the pNIPAM, in addition to the linear elastic law.

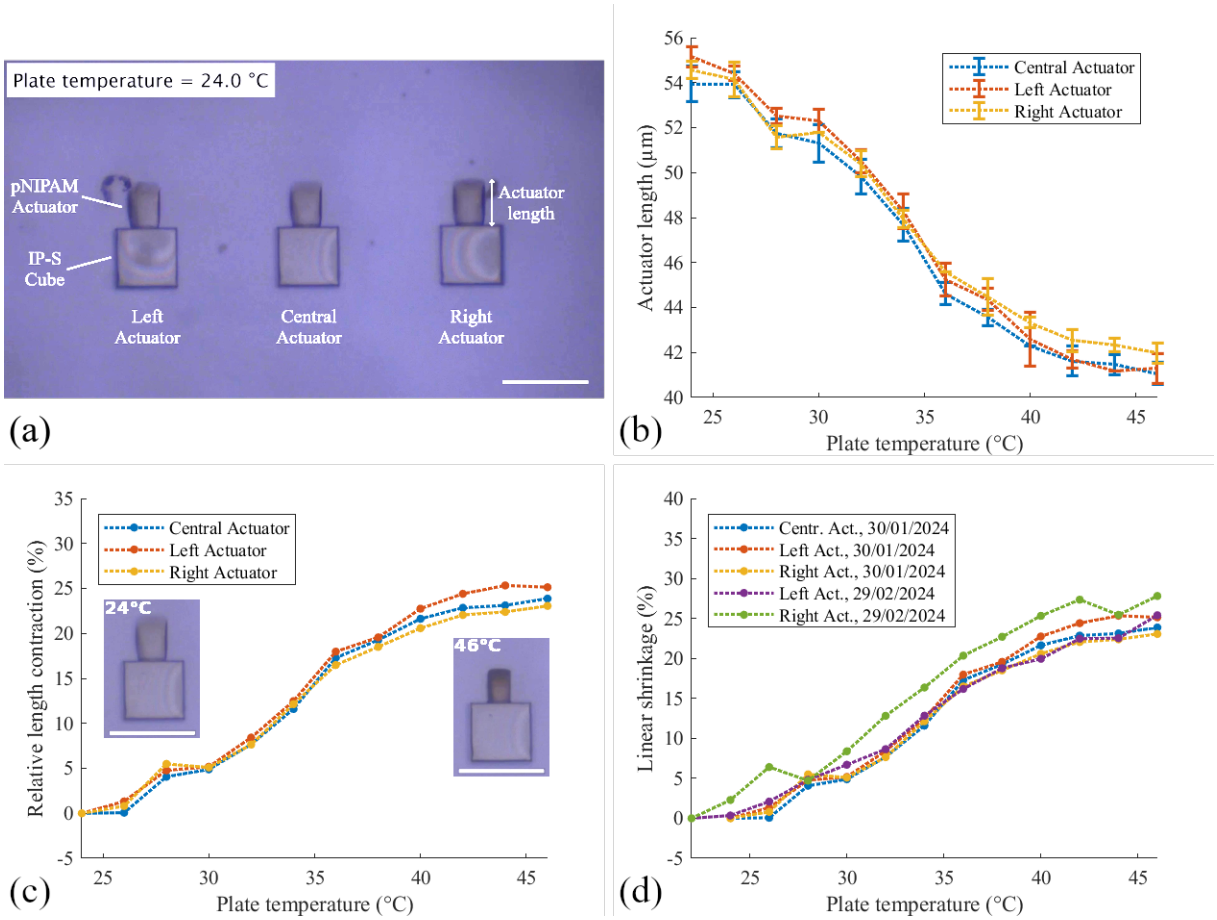

Fig. 4: Experimental measurement of the linear shrinkage of the fabricated pNIPAM actuators. (a) pNIPAM actuators used for the shrinkage measurements, Scale bar : 100 µm. (b) Length of the actuators with respect to the heating plate temperature. (c) Linear shrinkage of the actuators with respect to the heating plate temperature. (d) Comparison of the linear shrinkage between two prints, same printing parameters.

$$\frac{V(T_0)}{V(T)} = \frac{M}{m} + \frac{1 - \frac{M}{m}}{1 + e^{\frac{T - T_{inflexion}}{D}}} \tag{1}$$

With M and m the asymptotic value of the sigmoid function at high and low temperature respectively, $T_{inflexion}$ the inflexion point of the sigmoid and D a parameter tailoring the transition width. From the volumic ratio, the thermal strain ϵ_{th} and the evolution of the Young's modulus $E(T)$ with respect to the pNIPAM temperature can be retrieved with equation (2) and (3) [37], [38]:

$$\frac{V(T_0)}{V(T)} = \frac{1}{(\epsilon_{th} + 1)^3} \tag{2}$$

$$\frac{E(T)}{T}\frac{T_0}{E(T_0)} = \left(\frac{V(T_0)}{V(T)}\right)^n \tag{3}$$

With E_0 and n specific parameters of the relation between Young's Modulus and the polymer volume ratio.

The constitutive law (1) of the pNIPAM was fitted on relative volumic ratio $\frac{V(T_0)}{V(T)}$ values calculated with the equation (2) from the contraction measurements of Fig. 4c in Matlab, to obtain the $\frac{M}{m}$, $T_{inflexion}$ and D values reported in Table I, with a coefficient of determination $R^2 = 0.9839$. E_0 and n were deduced from the mechanical measurements of pNIPAM printed at 30 mm/s done by Spratte et al. [39], which use a similar pNIPAM resin formulation (the difference is the addition of PVP in our formulation) and had a similar contraction value.

$\frac{M}{m}$	$T_{inflexion}$	D	E_0	n
2.3	35.5 °C	2.9 °C	19 kPa	2.98

TABLE I: Values of parameters used in the FEM model of the pNIPAM actuator.

D. Experimental setup

To actuate the printed mechanism, the same global heating setup was used for all the presented experiments (Fig. 3). The heating of the devices was done in their storage water bath with a heating/cooling element (Cole-Parmer IC20 C-P). A CMOS camera (Imaging Source DFK 37BUX178) mounted on a microscope (Mitutoyo M Plan Apo. 7.5X/0.21 objective, with an Optem ZOOM 70XL optical tube) was used to acquire images of the devices under heating. A manual XYZ stage allowed to move the microscope. The driving of the heating plate and the recording of its temperature (1 measurement per second) was done with Matlab, while the recording of the camera images (30 FPS) was done with Open Broadcaster Software[1]. Image processing in Matlab was used for all the measurements reported in this paper unless specified otherwise.

III. STUDY STATIC BEHAVIOR OF THE PNIPAM ACTUATOR

A. Free displacement study

The free deformation of the actuator along their length according to temperature was experimentally studied with three $45 \times 30 \times 30$ μm pNIPAM cantilever beams as actuators, printed on $75 \times 75 \times 75$ μm IP-S cubes, as depicted in Fig. 4a. A noticeable swelling of the pNIPAM actuators was observed at the end of the actuator printing, with their length reaching 55 µm after development.

To measure the shrinkage of the actuators relative to temperature, the three beams were heated between 24°C and 46°C by 2°C steps, each step lasting 5 minutes. At the end of each step, 10 frames were extracted and used to measure the length of each beam (Fig. 4b). A 25% contraction of the beam was observed, following a sigmoidal evolution relative to temperature (Fig. 4c). This is in line with previous work on pNIPAM [20], [21]. The pNIPAM actuator also displayed a linear contraction span between 30°C and 40°C, which could be useful for the accurate position control of a soft microrobot.

Two supplementary actuators were printed one month later with a new batch of pNIPAM resin, using the same printing parameters and with the same dimensions. The shrinkage of the beam was very similar between all pNIPAM beams (Fig. 4d) whatever their print date, showing a good repeatability of the fabrication process.

B. Study of the actuator behavior under load

The behavior of the pNIPAM actuator under load was studied via Finite Element Modelling. The model was first validated in the free displacement case on the two supplementary actuators, since they were not used to fit the model's parameters. The FEM was used to simulate a $55 \times 30 \times 30$ μm pNIPAM actuator (to take into account the post-print swelling of the actuators) in a cantilever configuration submitted to temperatures between 22°C and 46°C. The simulated length variation was compared to the experimental measurements of the two supplementary actuators. The experimental results and the simulated result were in accordance (Fig. 5). This gives us enough confidence in the model to extrapolate the force behavior of the actuator from it.

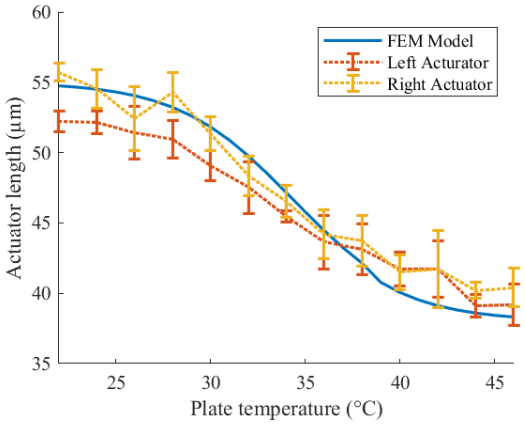

Fig. 5: Confrontation between simulated and measured actuator length in the free displacement case.

The force-displacement relation of the actuator was then studied, by simulating a $55 \times 30 \times 30$ μm pNIPAM actuator with a roller boundary condition at one end and a spring load at the other. By varying the spring stiffness, the force-displacement curve of the actuator was calculated for several isotherms between 22°C and 46°C (Fig. 6a).

The case where the actuator displayed no displacement was also studied to get an idea of the maximum force that can be expected. For this case, a $55 \times 30 \times 30$ μm pNIPAM actuator with roller boundary condition at both ends to fix the length of the actuator was simulated. The force generated by the actuator was calculated for temperatures between 22°C and 46°C (Fig. 6b).

At 45 °C, the model predicts a maximum force of 166 μN, one order of magnitude higher than the forces reported in the literature for pNIPAM actuators (10.3 μN in [34]) or other hydrogels (34 μN in [32]). However, the values reported in the literature were measured with elastic beam-based protocols (the hydrogel deforms a beam in a passive material supposed elastic, and the displacement is converted into force based on the stiffness of the beam). Since a displacement is present, the measured actuator force in this kind of protocol would be lower according to

[1]https://obsproject.com/

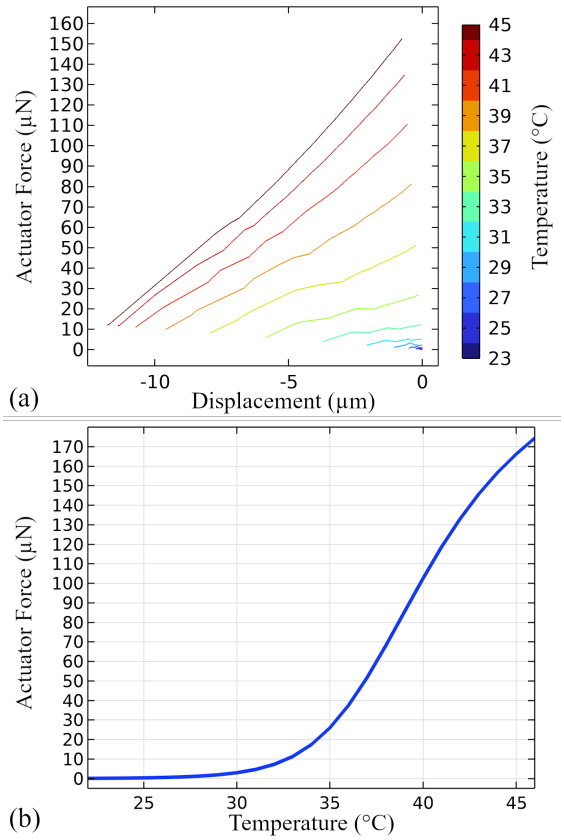

Fig. 6: FEM study of the actuator behavior under load conditions for the spring-load (a) and the null displacement (b) case. (a) Force-displacement relation of the actuator at several isotherms. (b) Maximum forces obtained for a null displacement with respect to temperature.

Fig. 6a. Indeed, when the simulated force values of the proposed actuator at 45 °C (Fig. 6a) are compared to the measure of Özkale et al. [34] for a similar displacement, similar values of force are obtained (respectively 10.3 μN for a 20% displacement and 12 μN for a 21% displacement). These results show an interesting behavior of the pNIPAM actuator in force: the actuator can be very delicate if allowed to move, but with one order of magnitude greater forces under its belt.

IV. Demonstration

A. Bi-material soft microrobot with a RR serial architecture

A RR soft microrobot design (classic robot design with two revolute joints in series) is proposed to demonstrate rotational movement with large amplitude. The robot is composed of two links and a base attached to the glass substrate, with two $40 \times 25 \times 5$ μm beams joint acting as revolute joints and two $45 \times 30 \times 30$ μm pNIPAM actuators. It was fabricated following the proposed approach. Each prototype was heated between 22°C and 46°C, by steps of 2°C and 5 minutes duration. The results are shown in Fig. 7.

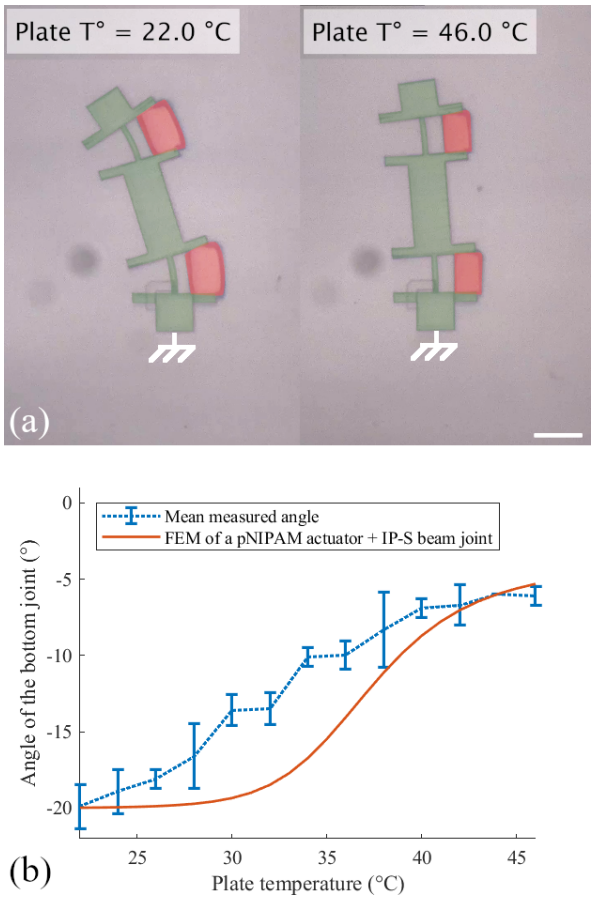

Fig. 7: Study of an RR soft microrobot behavior under heating. (a) RR microrobot at 22°C and 46°C, with the IP-S flexible mechanism and the pNIPAM actuators highlighted in green and red respectively, Scale bar: 50 μm. (b) Confrontation between the measured angular displacement and FEM simulations of a pNIPAM actuator actuating an IP-S flexible beam joint.

The angular displacement of the bottom joint was measured via image processing in Matlab. A 14° maximal angular displacement was measured (Fig. 7b), which is comparable to the best of the state-of-the-art [32]. The angular displacement observed is directly related to the temperature of the bath, showing that the microrobot is easily controllable. The RR soft microrobot also shows that this fabrication method can produce multi-actuator soft microrobots at the 100 μm scale, thus allowing a potential separated heating of the two actuators. The repeated tests demonstrate that pNIPAM actuators are strongly attached to the IP-S structures, an essential condition for making functional robots.

It can be noticed that the system displays an actua-

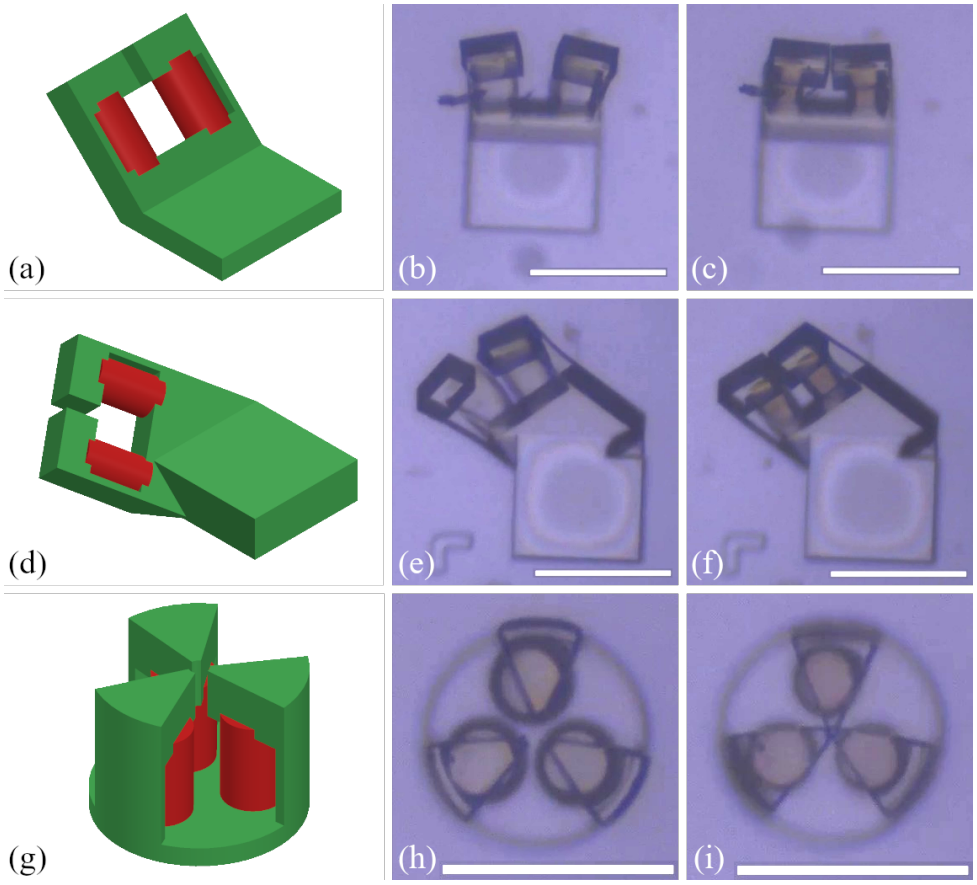

Fig. 8: 3D grippers CAD and their actuation at 22°C and 46°C respectively. In the CAD, the IP-S flexible mechanism is in green and the pNIPAM actuators are in red. (a), (b) and (c) Flat gripper rotated around one axis. (d), (e) and (f) Flat gripper rotated around two axis. (g), (h), (i) 3-jaw mandrel-like gripper. All scale bars are 100 μm.

tion even at low temperatures, which is not the result expected by the FEM (Fig. 6, Fig. 7b). A behavior like this would be expected if the revolute joint had no stiffness, causing a free rotational movement. However, this observation can be explained by the viscoelastic behavior of the IP-S: since the conducted experiment is in the timescale of minutes (each temperature plateau was sustained 5 minutes before angular measurements, to ensure that the system is at equilibrium), the viscous effect is taking place in the IP-S beam joint, allowing the flexible joint to slowly deform until no more force is applied by the pNIPAM actuator.

As a demonstration of the 3D capability of the fabrication approach, 3 designs of 100 μm 3D grippers (Fig. 8a,d, and g) with different integrated actuators (one per finger) are proposed: a flat gripper rotated around one axis, a flat gripper rotated around two axis, and a 3-jaw mandrel-like gripper ($40 \times 25 \times 5$ μm beams joint were used with $45 \times 30\varnothing$ μm pNIPAM actuators). All the designs are conveniently obtained after the fabrication process and observed under an optical microscope. The heating of the microgrippers between 22°C and 46°C confirmed their capacity to be actuated as shown in Fig. 8b, c, e, f, h, and i, with an initial gap estimated with ImageJ around 25 µm for Fig. 8b and a full closure of all the grippers.

V. CONCLUSION AND PERSPECTIVES

Bi-material 3D printed soft microrobots are proposed in this work, combining flexible mechanisms made from IP-S with integrated actuators made from pNIPAM. A static characterization of pNIPAM as an actuator was performed in free displacement via experimentation and under load via Finite Element Modelling.Then, a RR bi-material soft microrobot was designed and fabricated to study the behavior of multi-material 3D printed soft microrobots. One of the actuated R-joint was characterized, showing a 14° rotation range and a controllable motion in position when varying the temperature in a restrained range (22°C to 46°C). The bi-material manufacturing of the IP-S mechanism and pNIPAM actuators was then demonstrated on 3 designs of 3D microgrippers. The closing of each gripper is observed when the

temperature is controlled between 22°C and 46°C. The pNIPAM actuators showed promising behavior in force during the finite element analysis, which should be confirmed by further experimental validation. The bimaterial strategy could be used with different combinations of passive and active polymers with various stimuli. The proposed approach is an interesting base to make multi-DoF microrobots in the future, and paves the way to achieve complex 3D soft microrobots with large motions and an easily controllable actuation.

REFERENCES

[1] D. Felekis, *et al.*, "Quantifying growth mechanics of living, growing plant cells in situ using microrobotics," *Micro & Nano Letters*, vol. 6, no. 5, p. 311, 2011.

[2] K. Sakamoto, *et al.*, "Intuitive Cell Manipulation Microscope System with Haptic Device for Intracytoplasmic Sperm Injection Simplification," *Sensors*, vol. 24, no. 2, Jan. 2024, Art. no. 711.

[3] P. Saketi, *et al.*, "A flexible microrobotic platform for handling microscale specimens of fibrous materials for microscopic studies," *Journal of Microscopy*, vol. 248, no. 2, pp. 163–171, Nov. 2012.

[4] Y. Takeichi, *et al.*, "Micromanipulation and Pick-Up System for X-Ray Diffraction Characterization of Micrometer-Sized Single Particles," *Journal of Physics: Conference Series*, vol. 502, Apr. 2014, Art. no. 012008.

[5] M. Majda, *et al.*, "Cellular Force Microscopy to Measure Mechanical Forces in Plant Cells," in *Plant Cell Morphogenesis*, F. Cvrčková and V. Žárský, Eds. New York, NY, USA: Springer New York, 2019, vol. 1992, pp. 215–230.

[6] H. McClintock, *et al.*, "The milliDelta: A high-bandwidth, high-precision, millimeter-scale Delta robot," *Science Robotics*, vol. 3, no. 14, Jan. 2018, Art. no. eaar3018.

[7] M. Leveziel, *et al.*, "MiGriBot: A miniature parallel robot with integrated gripping for high-throughput micromanipulation," *Science Robotics*, vol. 7, no. 69, Aug. 2022, Art. no. eabn4292.

[8] C. J. Nwafor, *et al.*, "The Caturo: A Submillimeter Diameter Glass Concentric Tube Robot with High Curvature," *Advanced Intelligent Systems*, vol. 5, no. 2, 2023, Art. no. 2200308.

[9] Z. Xing, *et al.*, "A Super-Lightweight and Soft Manipulator Driven by Dielectric Elastomers," *Soft Robotics*, vol. 7, no. 4, pp. 512–520, Aug. 2020.

[10] S. H. Yang, *et al.*, "Microelectromechanical systems based Stewart platform with sub-nano resolution," *Applied Physics Letters*, vol. 101, no. 6, Aug. 2012, Art. no. 061909.

[11] N. Mamat, *et al.*, "Multiphysics & Parallel Kinematics Modeling of a 3DOF MEMS Mirror," *MATEC Web of Conferences*, vol. 32, Jan. 2015, Art. no. 01004.

[12] S. I. Moore and S. O. R. Moheimani, "A switched actuation and sensing method for a MEMS electrostatic drive," in *American Control Conference*, July 2016, pp. 5817–5822.

[13] K. Suzumori, *et al.*, "Applying a flexible microactuator to robotic mechanisms," *IEEE Control Systems Magazine*, vol. 12, no. 1, pp. 21–27, Feb. 1992.

[14] S. Kawata, *et al.*, "Finer features for functional microdevices," *Nature*, vol. 412, no. 6848, pp. 697–698, Aug. 2001.

[15] P. Mainik, *et al.*, "Recent Advances in Multi-Photon 3D Laser Printing: Active Materials and Applications," *Advanced Materials*, vol. 36, no. 11, 2024, Art. no. 2310100.

[16] G. Adam, *et al.*, "4D Printing: Enabling Technology for Microrobotics Applications," *Advanced Intelligent Systems*, vol. 3, no. 5, 2021, Art. no. 2000216.

[17] M. R. Lee, *et al.*, "Shape-Shifting 3D Protein Microstructures with Programmable Directionality via Quantitative Nanoscale Stiffness Modulation," *Small*, vol. 11, no. 6, pp. 740–748, Feb. 2015.

[18] T.-Y. Huang, *et al.*, "Four-dimensional micro-building blocks," *Science Advances*, vol. 6, no. 3, Jan. 2020, Art. no. eaav8219.

[19] M. Hippler, *et al.*, "Controlling the shape of 3D microstructures by temperature and light," *Nature Communications*, vol. 10, no. 1, Jan. 2019, Art. no. 232.

[20] G. Decroly, *et al.*, "A Voxel-Based Approach for the Generation of Advanced Kinematics at the Microscale," *Advanced Intelligent Systems*, vol. 5, no. 7, Mar. 2023, Art. no. 2200394.

[21] C. Deng, *et al.*, "Femtosecond Laser 4D Printing of Light-Driven Intelligent Micromachines," *Advanced Functional Materials*, vol. 33, no. 11, 2023, Art. no. 2211473.

[22] T. Watanabe, *et al.*, "Photoresponsive Hydrogel Microstructure Fabricated by Two-Photon Initiated Polymerization," *Advanced Functional Materials*, vol. 12, no. 9, pp. 611–614, Sept. 2002.

[23] D. Jin, *et al.*, "Four-dimensional direct laser writing of reconfigurable compound micromachines," *Materials Today*, vol. 32, pp. 19–25, Jan. 2020.

[24] M. A. Haq, *et al.*, "Mechanical properties of PNIPAM based hydrogels: A review," *Materials Science and Engineering: C*, vol. 70, pp. 842–855, Jan. 2017.

[25] N. Amdursky, *et al.*, "Elastic serum-albumin based hydrogels: mechanism of formation and application in cardiac tissue engineering," *Journal of Materials Chemistry B*, vol. 6, no. 35, pp. 5604–5612, 2018.

[26] P. Curie, "Sur la symétrie dans les phénomènes physiques, symétrie d'un champ électrique et d'un champ magnétique," vol. 3, no. 1, pp. 393–415, 1894.

[27] C. Xin, *et al.*, "Light-triggered multi-joint microactuator fabricated by two-in-one femtosecond laser writing," *Nature Communications*, vol. 14, no. 1, July 2023, Art. no. 4273.

[28] H. Zeng, *et al.*, "Light-Fueled Microscopic Walkers," *Advanced Materials*, vol. 27, no. 26, pp. 3883–3887, 2015.

[29] D. Martella, *et al.*, "Photonic Microhand with Autonomous Action," *Advanced Materials*, vol. 29, no. 42, Nov. 2017, Art. no. 1704047.

[30] L. Tan and D. J. Cappelleri, "Design, Fabrication, and Characterization of a Helical Adaptive Multi-Material MicroRobot (HAMMR)," *IEEE Robotics and Automation Letters*, vol. 8, no. 3, pp. 1723–1730, Mar. 2023.

[31] Y. Lee, *et al.*, "Multifunctional 3D-Printed Pollen Grain-Inspired Hydrogel Microrobots for On-Demand Anchoring and Cargo Delivery," *Advanced Materials*, vol. 35, no. 10, Jan. 2023, Art. no. 2209812.

[32] Z.-C. Ma, *et al.*, "Femtosecond laser programmed artificial musculoskeletal systems," *Nature Communications*, vol. 11, no. 1, p. 4536, Sept. 2020.

[33] A. Nishiguchi, *et al.*, "In-Gel Direct Laser Writing for 3D-Designed Hydrogel Composites That Undergo Complex Self-Shaping," *Advanced Science*, vol. 5, no. 1, 2018, Art. no. 1700038.

[34] B. Özkale, *et al.*, "Modular soft robotic microdevices for dexterous biomanipulation," *Lab on a Chip*, vol. 19, no. 5, pp. 778–788, 2019.

[35] S. Henein, "Conception des structures articulées à guidages flexibles de haute précision," Ph.D. dissertation, Dept. Microtechnol., EPFL, Lausanne, Switzerland, 2000.

[36] D. E. Marschner, *et al.*, "A methodology for two-photon polymerization micro 3D printing of objects with long overhanging structures," *Additive Manufacturing*, vol. 66, Mar. 2023, Art. no. 103474.

[37] G. L. Puleo, *et al.*, "Mechanical and rheological behavior of pNIPAAM crosslinked macrohydrogel," *Reactive and Functional Polymers*, vol. 73, no. 9, pp. 1306–1318, Sept. 2013.

[38] K. S. Anseth, *et al.*, "Mechanical properties of hydrogels and their experimental determination," *Biomaterials*, vol. 17, no. 17, pp. 1647–1657, Jan. 1996.

[39] T. Spratte, *et al.*, "Increasing the Efficiency of Thermoresponsive Actuation at the Microscale by Direct Laser Writing of pNIPAM," *Advanced Materials Technologies*, vol. 8, no. 1, 2023, Art. no. 2200714.